Journal of Robotics and Control (JRC)
Volume 6, Issue 3, 2025
ISSN: 2715-5072, DOI: 10.18196/jrc.v6i3.24778 

# Improved Horizon Calculation and Performance Comparison of I-UFIR and Filtering Techniques for Baseline Wander Removal in ECG Signals

Roberto Olivera-Reyna [1], Reynel Olivera-Reyna [2], Osbaldo Vite-Chavez [3], Rosa J. Perez-Chimal [4], Jorge U. Muñoz-Minjares [5*]
[1, 2, 4] Posgrado en Ingeniería para la Innovación Tecnológica, Universidad Autónoma de Zacatecas, Ramón López Velarde 801, Zacatecas, México
[3, 5] Unidad de Ingeniería Eléctrica, Universidad Autónoma de Zacatecas, Campus Jalpa, Libramiento Jalpa, Km 156+380 Fracc. Solidaridad Jalpa, Zacatecas, México
Email: [1] roliverar@uaz.edu.mx, [2] reynel@uaz.edu.mx, [3] osvichz@uaz.edu.mx, [4] r.perez@uaz.edu.mx, [5] ju.munoz@uaz.edu.mx
*Corresponding Author

***Abstract*—Removing Baseline Wander (BLW) is crucial in ECG signal filtering without altering its morphology, as BLW can hide critical diagnostic features such as ST-segment deviations, T-wave changes, and P-wave morphology. These distortions can lead to misinterpretations of the ECG, potentially resulting in incorrect diagnoses or missed clinical conditions, such as myocardial ischemia or arrhythmias. In this study, the term optimal is defined by the ability of methods to effectively remove baseline wander while preserving the key morphological features of the ECG signal, such as the ST-segment, T-wave, and P-wave, with minimal distortion. Some algorithms with minimal information and tuning offer acceptable BLW approximations. This study applies the I-UFIR filter to remove BLW and compares its performance with the Savitzky-Golay (S-G) filter and Wavelet transform with 9 and 10 decompositions. The Savitzky-Golay (S-G) filter was chosen for its effectiveness in smoothing baseline wander while maintaining the original morphology of the ECG signal. Wavelet transform was selected for its multi-resolution analysis, which enables the separation of BLW from essential ECG features. To assess the performance of these methods, Mean Square Error (MSE), Root Mean Square Error, and box plot comparisons were used to quantify and visually analyze their effectiveness in baseline correction. Since determining the horizon for I-UFIR and S-G filters is challenging, two approaches are compared, first a traditional calculation and one based on the signal's sampling frequency. The comparison of these approaches for computing the optimal horizon can simplify BLW estimation, reducing both computational effort and time, as the traditional approach depends on iterative calculations. Furthermore, two ECG signal sources are used for testing, one synthetic and the other real acquired using the ECG sensor AD8232, ADC ADS1115, and microcontroller MEGA 2560. The AD8232 ECG sensor records the electrical signal of the heart, the ADS1115 ADC converts the analog signal into a digital form for processing, and the MEGA 2560 microcontroller coordinates data acquisition, ensuring precise and dependable ECG signal capture for analysis. However, it is important to note that the study is based on ECG signals obtained from a single individual under specific conditions and recorded using a particular hardware setup, which may limit the generalizability of the findings to a broader population or different ECG recording systems and environments. Wavelet decompositions yield the best results for synthetic signals, while I-UFIR and S-G filters perform better with real signals.***

***Keywords*—Baseline Wander; I-UFIR Filter; Horizon for BLW; Savitzky-Golay; Wavelet.***

## I. INTRODUCTION

According to the World Health Organization, non-communicable diseases (NCDs) cause 41 million deaths each year, accounting for 71% of global deaths. Each year, 17 million people under the age of 70 die from an NCD, with 86% of these deaths occurring in low and middle-income countries [1]. Cardiovascular diseases (CVDs) are responsible for most NCD-related deaths, with an estimated 17.9 million deaths annually, followed by cancer with 9.3 million, chronic respiratory diseases with 4.1 million, and diabetes with 2 million, including deaths due to diabetic nephropathy [2]-[6]. CVDs represent a group of heart and blood vessel disorders that include coronary heart disease, cerebrovascular disease, and rheumatic heart disease [7]-[10]. Accurate ECG readings are essential for diagnosing and managing CVDs, providing vital insights into the electrical activity of the heart. High quality ECG signals are key to detecting abnormalities, which makes improving ECG signal quality a crucial step in addressing the global burden of CVDs.

The electrocardiogram (ECG) is one of the most important clinical tools for diagnosing heart diseases, making the accuracy of the ECG crucial. The ECG signal is the electrical manifestation of the heartbeats over time, and this signal can be recorded under various conditions to detect different heart abnormalities [11]-[15]. The ECG signal consists of a P wave due to atrial depolarization, a QRS complex due to atrial repolarization and ventricular depolarization, and a T wave due to ventricular repolarization [16]-[20]. The P wave, QRS complex, and T wave are crucial components of the ECG signal, with each representing different phases of the electrical cycle of the heart. The P wave reflects atrial depolarization, the QRS complex corresponds to ventricular depolarization, and the T wave represents ventricular repolarization. So, an accurate detection of these segments is essential for diagnosing heart conditions like arrhythmias, myocardial infarction, and heart

block [21]-[24]. The abnormalities in these waves can indicate underlying cardiovascular issues. Fig. 1 shows an ECG signal from a healthy person, highlighting key components such as the P wave, QRS complex, and T wave. In contrast, Fig. 2, presented later in the manuscript, shows an ECG signal affected by Baseline Wander (BLW), demonstrating how BLW distorts the morphology of the signal and impacts diagnostic accuracy.

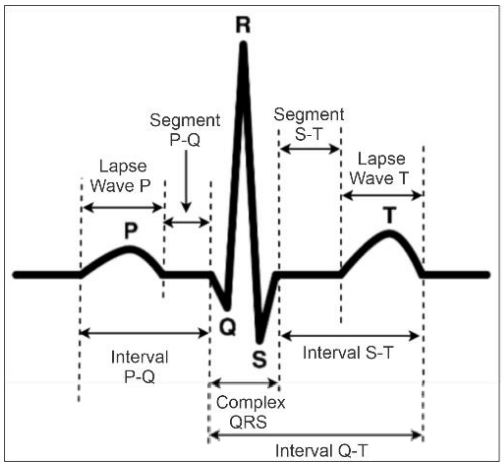


Fig. 1. Representation of a cardiac cycle with the waves and segments in an ECG signal

However, the quality of the ECG signal can degrade during the acquisition stage due to various interferences or noise, such as the 50 or 60 Hz frequency from the power line, artifacts caused by patient movement, and baseline wander (BLW) [25]-[28]. To address these challenges, effective baseline wander removal techniques in ECG signal preprocessing can improve the accuracy of cardiovascular disease diagnosis by preserving essential ECG features while mitigating signal distortion caused by noise and artifacts. All these factors could complicate the accurate identification of the elements that reflect the characteristics of the heart's physiological activity [29]-[32]. Consequently, an interference suppression or preprocessing stage should be applied before analyzing the electrocardiographic signal. One of the most important tasks in the preprocessing stage involves removing or correcting the baseline wander in the ECG signal [33]-[36]. Since BLW is a low-frequency fluctuation, this artifact can deform the true shape of the ECG record. Therefore, its presence can hide essential features like the ST-segment, T-wave, and P-wave, making the accurate diagnosis of cardiovascular conditions more difficult.

The nature of baseline wander in the ECG is not cardiac in origin. This artifact primarily arises from patient movement, the breathing process, and poor electrode-skin contact. As a result, it appears as a low-frequency artifact or noise, typically in the range of 0.5 to 0.6 Hz [37]-[40]. However, increased body movement caused by exercise or stress tests can cause the BLW frequency to vary from 0.05 to 3 Hz [41][42]. Baseline wander at the lower end of this range (0.05 to 0.5 Hz) is commonly linked to respiratory movements, while higher frequencies (0.5 to 3 Hz) are typically caused by muscle contractions or changes in sensor position due to physical activity. Due to various types of noise that can affect ECG acquisition, a preprocessing step is recommended to remove artifacts from the ECG signal before estimating the BLW. To address this issue, traditional techniques are employed, such as digital filtering, wavelet transform methods, and adaptive filtering techniques, which have been widely used for ECG signal denoising [43]-[45]. Fig. 2 shows the ECG signal from file 103 of the MIT-BIH Arrhythmia Database [46][47], which presents the BLW phenomenon. Fig. 2 illustrates how the low-frequency fluctuations mask the normal shape of the ECG measurements. In this particular case, the BLW modifies the ST-segment, making it difficult to accurately evaluate the condition of the heart, such as potential ischemia. This example highlights the challenge presented by the presence of BLW in clinical diagnostics, as it can hide critical features needed for accurate interpretation.

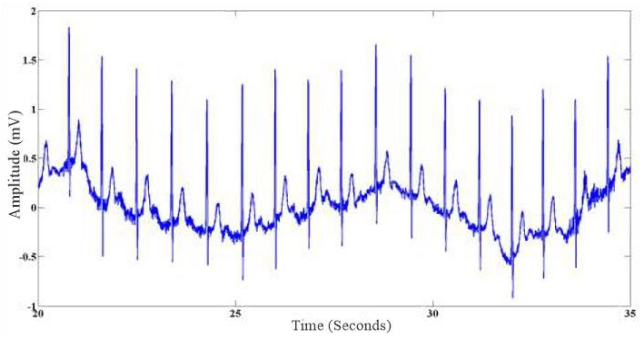


Fig. 2. ECG signal affected by Baseline Wander (BLW)

Given the significant impact of baseline wander on ECG interpretation, several filtering techniques have been developed to mitigate this issue while preserving the quality of the signal. In this work, these approaches can be categorized into digital filtering techniques, wavelet-based methods, and adaptive filtering strategies. First studies in [48]-[51], focus on different methods based on classical digital filtering techniques, such as FIR and IIR filters, for eliminating BLW. While these methods effectively reduce baseline wander, they often introduce signal distortion, particularly at lower frequencies, which can impair the accuracy of critical ECG features. These methods were evaluated using performance metrics including the Power Spectral Density (PSD), the Signal-to-Noise Ratio (SNR), and the Mean Square Error (MSE), but they may struggle with preserving morphological features of the ECG signal. Second, approaches based on wavelets have been explored in [52]-[55], where different wavelet levels and thresholding techniques were applied to ECG signals contaminated by various types of noise, including BLW. While wavelet-based methods have shown promising results in separating noise from the ECG signal, their effectiveness is highly dependent on the choice of decomposition levels and thresholding parameters, which can be difficult to optimize without prior knowledge of the signal characteristics. The goal of these studies was to identify the combination of decomposition levels and thresholding parameters that minimize distortion in the ECG signal while effectively removing BLW. However, the trade-off between noise removal and signal preservation remains a challenge. Third, adaptive filtering techniques have been investigated, particularly the Wiener Filter (WF) and the Kalman Filter (KF) [56]-[59]. These methods adapt to the characteristics of the signal and noise in

real-time, offering a more dynamic approach. In these works, it is compared the MSE, SNR, percentage difference in MSE, PSD, and spectrogram were used to compare the output of each filter, with the WF yielding better results. However, the performance of adaptive filters can be significantly impacted by the quality of the noise model and the computational cost, making them less practical for real-time applications in some cases. Additionally, in [60]-[62] have examined the performance of different IIR filters, such as Butterworth, Elliptic, Chebyshev I, and Chebyshev II. These methods were evaluated based on the SNR and a qualitative evaluation of their impact to the ECG signal. While these filters perform well in certain conditions, they may not be suitable for all types of ECG signals and can introduce phase distortion or require extensive parameter tuning. Each of the techniques described above requires prior knowledge of the ECG signal, an approximation model of the signal, a noise model, or extensive tuning to achieve the best results. The existing methods all have their strengths and weaknesses, but none are universally applicable across all types of ECG signals or clinical settings. The limitations of these techniques, such as their dependence on signal and noise models, their susceptibility to signal distortion, and the need for parameter tuning, highlight the need for more robust and adaptable solutions.

Regarding the evaluation metrics used in previous studies, PSD, SNR, and MSE are key indicators for assessing the effectiveness of baseline wander removal techniques. It is important to note that PSD provides insight into the frequency components of the signal, aiding in the evaluation of how well a method suppresses low-frequency BLW without altering essential ECG waves. The SNR measures the ratio of the desired ECG signal to background noise, reflecting the level of signal preservation after filtering. Meanwhile, MSE quantifies the difference between the filtered ECG signal and a reference clean signal, offering an objective assessment of signal distortion introduced by the BLW removal method. The selection of SNR, MSE, and PSD as evaluation metrics for BLW removal is important because they provide a comprehensive assessment of signal quality, accuracy, and frequency-domain characteristics. SNR ensures that the signal remains clear after BLW removal, MSE quantifies the deviation from the original signal to preserve waveform integrity, and PSD verifies that low-frequency noise has been effectively suppressed without distorting important ECG features.

The research contribution is significant as it demonstrates the effective implementation of I-UFIR and S-G filters in low-cost ECG acquisition systems, highlighting their potential to enhance the accuracy and stability of wearable health monitoring devices. The study shows that these filtering techniques yield improved performance, evidenced by narrower whiskers and median values closer to zero, while also being computationally efficient and adaptable to resource constrained hardware. This makes them well suited for real-time ECG signal processing in remote patient monitoring and medical diagnostics.

## II. STATE-SPACE MODEL, BASELINE WANDER, AND ESTIMATORS

### A. Polynomial Degree in the State-Space

The signal representation is carried out using a given polynomial degree in the state-space, which allows for an accurate description of the ECG signal within the defined time frame. It is clear that the selection of the polynomial degree plays a crucial role in modeling accuracy and filtering performance. A higher polynomial degree can better approximate baseline wander (BLW) by capturing more complex trends in the ECG signal. However, increasing the polynomial degree also introduces trade-offs, such as higher computational complexity, overfitting, and increased sensitivity to noise [63]. Once this is specified, the ECG signal can be represented within an interval of length $N$, where $m = n - N + 1$. It is important to note that the ECG signal is considered to be timeless and deterministic. Also, it is assumed that the measurement of the ECG signal is affected by zero-mean noise, whose standard deviation is unknown, and that follows a Gaussian distribution, although not necessarily. Under these conditions, the representation of an ECG signal is expressed as follows.

$$x_k = Ax_{k-1} + Bw_k \tag{1}$$

$$y_k = Cx_k + v_k \tag{2}$$

The state vector of the discrete-time system is denoted by $x_k \in R^K$, where $k$ is the time index, and $A$ represents the state transition matrix, which is used to project the state at the previous time step, $x_{k-1}$, to the current state $x_k$. In this context, $B$ is the matrix that models the system's noise. The measurement vector $y_k \in R^M$ is obtained through the observation matrix $C \in R^{M\times K}$, which maps the state $x_k$ to the measurements $y_k$ [64]-[66]. The process noise $w_k$is modeled as zero-mean white Gaussian noise, i.e., $w_k \sim N(0, Q_k) \in R^M$, where $Q_k$ represents its covariance matrix. Due to the significant time and resource requirements for testing with various noise types, we assume zero-mean Gaussian noise for consistency and controlled comparison of the proposed techniques, acknowledging that alternative noise models could be explored in future studies to assess their robustness in diverse scenarios. Similarly, the observation noise $v_k$is also considered white Gaussian noise with zero mean, i.e., $v_k \sim N(0, R_k) \in R^M$, and its covariance is given by $R_k$. It is assumed that the vectors $w_k$ and $v_k$, as well as the initial state, are independent of each other and uncorrelated at each instant. When considering the baseline wander $b_k$ in equation (2), this equation is defined as:

$$r_k = Cx_k + v_k + b_k = y_k + b_k. \tag{3}$$

The baseline wander is simulated by adding an inclined line to a sinusoidal signal [67]:

$$b_k = S + mk + Vcos(2\pi \frac{k}{T} + \phi), \tag{4}$$

the period of the sinusoid $T$ controls the severity of the baseline swing, $m$ controls the slope of the baseline wander, which can be represented as $m = tan(\theta)$. The selection of the parameters $\theta$ and $V$ in the baseline wander model is

crucial for accurately simulating real world baseline drift in ECG signals. The parameter θ determines the slope of the baseline wander, as it is related to m. A steeper slope, $\theta$ with a larger magnitude, results in a more pronounced drift over time, simulating conditions where gradual signal shifts occur due to patient movement or electrode instability. The appropriate value of $\theta$ depends on the expected baseline variations in clinical scenarios. Similarly, the parameter $V$ controls the amplitude of the sinusoidal component, which represents oscillatory baseline drift often caused by respiratory influences or body movement. A higher $V$ results in more significant deviations, whereas a lower $V$ simulates minor fluctuations. Selecting $V$ requires considering physiological variations observed in real ECG recordings to ensure realistic baseline wander characteristics. Finally, different values for $\phi$ allows the generation of different baseline wander sequences with similar characteristics. The polarization term $S$ is set such that the values of the sequence stay within the range.

Once the equations for the interpretation of the ECG signal are established, various algorithms for processing the ECG signal with wander can be described.

### B. *Maximal Overlap Discrete Wavelet Transform (MODWT)*

The Discrete Wavelet Transform (DWT) of a time series $X$ is now a well-known method for analyzing its characteristics at multiple scales [68]. However, there is a variation called the Maximal Overlap Discrete Wavelet Transform (MODWT). This variation discards orthogonality, as it does not perform downsampling, in order to achieve characteristics such as translation invariance and the ability to analyze a time series with an arbitrary sample size [69][70]. By avoiding subsampling, MODWT preserves the temporal resolution of the signal while accommodating arbitrary sample sizes. This characteristic makes it particularly useful for ECG signal analysis, as it effectively estimates baseline wander noise through multi-resolution decomposition, enhancing the accuracy of further processing steps such as feature extraction and noise removal.

Now, let $\{\tilde{h}_1\} \equiv \{\tilde{h}_{1,0,\dots}\, \tilde{h}_{1,L-1}\}$ be the wavelet filter coefficients of a family of Daubechies wavelets with compact support [71], and let $\{\tilde{g}_1\} \equiv \{\tilde{g}_{1,0,\dots}\, \tilde{g}_{1,L-1}\}$ be the corresponding scaling filter coefficients, defined by the quadrature mirror relation $\tilde{g}_{1,m} = (-1)^{m+1}\, \tilde{h}_{1,L-1-m}$.

The wavelet filter $\tilde{h}_1$ is associated with a unit scale, normalized in such a way that $\sum \tilde{h}_1{}^2 = 1/2$, and it is orthogonal to its even shifts. For any sample of size $N \geq L$ and with $h_{1,m} = 0$, let

$$\widetilde{H}_{1,k} = \sum_{m=0}^{N-1} \quad \tilde{h}_{1,m}\ e^{-\frac{i2\pi mk}{N}},\ k = 0, \dots, N-1, \tag{5}$$

Let the Discrete Fourier Transform (DFT) of $\{\tilde{h}_1\}$, and let $\tilde{G}_{1,k}$ denote the DFT of $\{\tilde{g}_1\}$. Now, the wavelet filter $\{\tilde{h}_j\}$ for the scale $\lambda_j \equiv 2^{j-1}$ is defined as the inverse DFT of

$$\widetilde{H}_{1,k} = \widetilde{H}_{1,2^{j-1}k \bmod N} \prod_{l=0}^{j-2} \quad \tilde{G}_{1,2^l k \bmod N} \tag{6}$$

where $k = 0, \dots N-1$. The wavelet filter associated with the scale $\lambda_j$ has a length of $min\{N, L_j\}$, where $L_j \equiv (2^j - 1)(L-1) + 1$. Additionally, the scaling filter $\{\tilde{g}_J\}$ for the scale $2\lambda_J$ is defined as the inverse DFT of

$$\tilde{G}_{J,k} = \prod_{l=0}^{J-2} \quad \tilde{G}_{1,2^l k \bmod N}, \quad k = 0, \dots, N-1 \tag{7}$$

In order to construct the partial-order Maximal Overlap Discrete Wavelet Transform of order $j$, it is assumed that $\{\chi_k\} \equiv \{\chi_{0,} \cdots, \chi_{N-1}\}$ is the DFT of $X$ for an arbitrary value of $N$. The MODWT coefficient vector $\widetilde{W}_j, j = 1, \dots, J$ is defined as the inverse DFT of $\{\widetilde{H}_{j,k}\, \chi_k\}$ and is associated with changes at scale $\lambda_j$. Similarly, the scaled MODWT coefficient vector $\tilde{V}_J$ is defined by the inverse DFT of $\{\tilde{G}_{J,k}\, \chi_k\}$, and it is associated with averages at scale $2\lambda_J$ and higher. For dyadic-length time series, the MODWT can be downsampled and rescaled to obtain an orthonormal DWT. Thus, the MODWT coefficients can be interpreted as weighted mean differences of the original observations. For this work, a Multi-Resolution Analysis (MRA) of the MODWT matrix will be used, with its parameters defined later.

### C. *I-UFIR Filter*

The filter known as the Iterative Unbiased Finite Impulse Response (I-UFIR) is obtained through a recursive process of the UFIR filter in its block version, which is carried out in two main phases, prediction and update [64,65]. This method does not require prior information about the statistics or the initial conditions of the process. In the I-UFIR algorithm, the estimation is performed iteratively using the variable $l$, which starts at $l = m + K$ and ends at $l = k$. The I-UFIR filter operates with a set of measurements $N$, which is a time interval defined by the horizon $[m, k]$, ranging from $[m = k - N + 1]$ to $k$. Therefore, the parameter $N$ is commonly referred to as the horizon or window. This algorithm also requires knowledge of the previous state estimate

$$\hat{x}_l^- = A\hat{x}_{l-1}^-, \tag{8}$$

for the known previous state $\hat{x}_{l-1}^-$, this approach avoids considering the previous covariance error. During the update phase, the I-UFIR algorithm performs a recalculation of the Generalized Noise Power Gain (GNPG) $G_l$ as follows:

$$G_l = [C^T C + (AG_{l-1}A^T)^{-1}]^{-1}, \tag{9}$$

this equation is derived from $G_l = \left(W_{m,j}^T, W_{m,l}\right)^{-1}$, where $W_{m,l}$ is the UFIR filter gain [64]. The equation (9) quantifies how the filtering process influences the noise present in the signal. Specifically, it measures the amplification or attenuation of noise as the filter operates over a given window size $N$. A larger $N$ enhances noise suppression by incorporating more past observations but may introduce a trade-off, causing response lag and reducing adaptability to rapid signal changes.

The residuals of the measurements can be defined as

$$z_l = y_l - Cx_l^-, \tag{10}$$

The bias gain adjustment is obtained by

$$K_l = G_l C^T \tag{11}$$

and the estimated state is

$$\hat{x}_l = \hat{x}_l^- + K_l z_l. \tag{12}$$

The bias gain adjustment $K_l$ plays a key role in controlling the adaptive nature of the filter during this iterative refinement. After obtaining the estimate $\hat{x}_l$, its smoothing is carried out through a simple projection over the interval $l - q$, using the system matrix as follows

$$\hat{x}_{l-q} = A^{-q} - \hat{x}_l. \tag{13}$$

According to the suggestions made in [72], to tune the I-UFIR filter, we set $l = 2$ and define $p = -q$ as follows

$$p = \lfloor -\frac{N-1}{2} - \frac{1}{2}\sqrt{\frac{N^2+1}{5}} \rfloor \tag{14}$$

By setting $l = 2$ and defining $p$, the I-UFIR filter adapts its characteristics to balance denoising with preserving the important features of the ECG signal, ensuring effective baseline wander removal.

Given the nature of the I-UFIR algorithm in its smoothing modality, the initial values of $\hat{x}_{l-q}$ are set to zero until the sample at $N + 1$ is reached. This approach ensures that the filter gradually accumulates sufficient data within the predefined window size $N$ before producing meaningful estimates, preventing distortions caused by insufficient initial information. A pseudo-code of the iterative UFIR algorithm proposed by [64] is presented in Algorithm 1. Here, it is detailed the I-UFIR filter proposed by [64] in the form of pseudo-code.

| **Algorithm 1.** Pseudocode I-UFIR |
|---|
| **Input Parameters.**<br>$r_k$: Measurement data,<br>$N$: Window size (determines how many past observations are considered)<br>$q$: Smoothing interval (defines how far back the smoothing extends) |
| **Results**: $\hat{x}_k$ Estimated state at time step k |
| 1: **Begin** : |
| 2: **for** $k = N - 1, N, \ldots$ **do** |
| 3: $m = k - N + 1, s = k - N + K$ |
| 4: $G_s = \left(W_{m,s}^T, W_{m,s}\right)^{-1}$ Compute Initial Gain |
| 5: $\tilde{x}_l^- = G_s W_{m,s}^T Y_{m,s}$ Compute Initial State Estimate |
| 6: **for** $l = s + 1$ **to** $k$ |
| 7: $\tilde{x}_l^- = A\tilde{x}_{l-1}^-$ Predict the state, eq. (5) |
| 8: $G_l = [C^T C + (AG_{l-1}A^T)^{-1}]^{-1}$ Update (GNPG), eq. (6) |
| 9: $K_l = G_l C^T$ Compute bias gain adjustment, eq. (8) |
| 10: $\tilde{x}_l = \tilde{x}_l^- + K_l z_l$ Correct the state estimate, eq. (9) |
| 11: **end for** |
| 12: $\hat{x}_k = \tilde{x}_l$ Store the final state estimate |
| 13: $\hat{x}_{k-q} = A^{-q}\hat{x}_k$ Apply Smoothing Step, eq. (10) |
| 14: **end for** |

*D. Suavizador Savitzky-Golay*

The *Savitzky-Golay* (S-G) smoother was used due to its similarity to working with a horizon $N$, like the I-UFIR filter. The S-G algorithm, also known as the least squares smoothing filter, was designed to retain high-frequency components in a signal while eliminating both noise and the average filter [73, 74]. The approach was originally developed in [75] and has since been widely applied to smooth various noisy signals.

Mathematically, the S-G filter is based on a local polynomial least-squares approximation within a moving window of length $N$. For each window, a polynomial of degree $d$ is fitted to the data using a least-squares criterion, with the central value of the polynomial serving as the filtered output. The filter coefficients are derived by solving a linear system that minimizes the squared error between the polynomial and the data. With a fixed horizon $N$, the S-G filter effectively balances noise suppression and feature preservation, making it particularly suitable for ECG signal processing, as it preserves high-frequency components, such as QRS complexes, without significant phase distortion.

In this work, we employ the generalized form of the S-G smoother described in [73], with respect to a polynomial of degree $d$ and a moving window of $N$ points. A pseudo-code for the S-G smoother is shown in Algorithm 2, and the output $\hat{x}_{SG}$ represents the S-G estimate. The polynomial smoothing filter of length $N$ and order $d$ has been implemented with a function $sg$, represented by the symbol $S$ in Algorithm 2, and is described in detail in [73].

| **Algorithm 2.** Pseudocode of Savitzky-Golay |
|---|
| **Input Parameters**: $d, N, r_k$ |
| **Results**: $\hat{x}_{SG\|k}$ |
| 1: **Begin**: |
| 2: $M = (N - 1)/2$ |
| 3: $[L, L_1] = size(y_k)$ |
| 4: $S = sg(d, N)$ Length of $N$ of order $d$. |
| 5: $for\ i = 1\ to\ M + 1\ do$ Input transients |
| 6: $\hat{x}_i = S_i^T * y_{n\|N}$ |
| 7: **end for** |
| 8: **for** $n = M + 2\ to\ L - M - 1$ **do** Stable State. |
| 9: $\hat{x}_k = S_{M+1}^T * y_{n-M:n+M}$ |
| 10: **end for** |
| 11: **for** $i = 0$ **to** $M$ **do** Input and Output transients |
| 12: $\hat{x}_{L-M+i} = S_{M+1+i}^T * y_{L-N+1:L}$ |
| 13: **end for** |

It can now be observed that both the I-UFIR smoothing algorithm and the S-G smoothing algorithm share the same mathematical origin based on the discrete convolution. However, the S-G smoother was developed only for even-order polynomials with a fixed delay $q = N/2$, while the I-UFIR algorithm does not impose such restrictions and is therefore more general.

*E. Characteristics Comparison of Algorithms*

The I-UFIR filter, MODWT, and S-G smoother each offer distinct advantages for ECG signal processing. The I-UFIR filter is notable for its versatility—functioning as a

smoother, filter, or predictor—and can be easily adjusted using the parameters $l$ and $p$. It does not require a strict Gaussian noise assumption, making it effective in diverse noise conditions while ensuring waveform integrity. In contrast, MODWT excels in multi-resolution analysis by efficiently separating baseline wander across different frequency bands, though it assumes stationary noise and has higher computational complexity. The S-G smoother employs polynomial-based filtering, controlling smoothness through window size and polynomial degree, and is particularly effective at preserving high-frequency ECG features, such as QRS complexes, despite assuming smooth noise variations.

The computational complexity of these techniques varies considerably. The I-UFIR filter exhibits moderate to high complexity due to its iterative and recursive operations, while MODWT is computationally intensive because of the multi-resolution analysis and processing required for multiple decomposition levels. The S-G smoother, based on local polynomial least-squares fitting within a moving window, offers lower computational complexity, making it more efficient in scenarios with limited computational resources.
In summary, each method presents distinct strengths, making them suitable for specific ECG processing applications depending on noise conditions and signal preservation requirements.

## III. MATERIALS AND METHODS

Fig. 3 shows the methodology proposed in this work. In the stage that contains the unprocessed ECG signal, there is the synthetic ECG signal, to which the baseline wander artifact is added. The generation of the synthetic signal and the acquisition of the real signal are explained in detail in the following subsections.

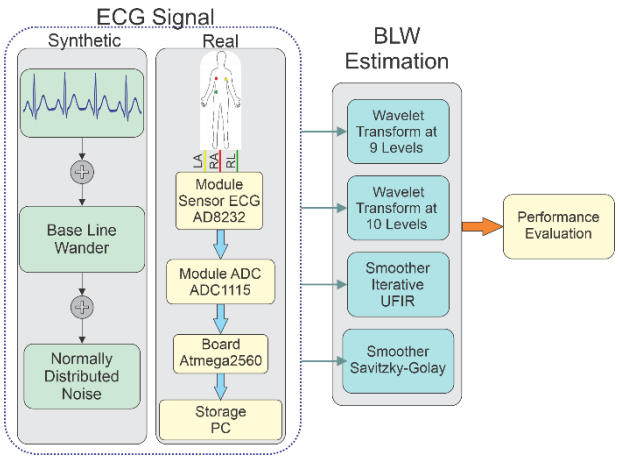


Fig. 3. ECG Signal Simulation Stages for BLW Estimation Comparison: Synthetic Signal, Synthetic Signal with BLW and Gaussian Noise, and BLW Estimation with Different Algorithms

### A. Synthetic Signals

To generate the synthetic signal, it is proposed to use the function developed in [76], which simulates ECG signals using different parameters, such as sampling frequency, approximate number of beats, noise, mean heart rate, among others. In Fig. 3, a general overview is provided of how a synthetic signal is obtained. First, the *ecgsyn* function is used to generate a simulated ECG signal that contains the main waves of a PQRST complex. Next, a baseline wander signal is simulated using equation (4), which is then added to the simulated ECG signal. Finally, the signal is added to normally distributed noise to simulate some of the artifacts that can affect an ECG signal during its acquisition. Each of the parameters used in this stage will be presented in detail in the subsection on Algorithm Performance on Synthetic Signals.

### B. ECG Signal Acquisition Circuit Units

The ECG signal acquisition circuit suggested is based on a connector cable with three adhesive electrodes, an AD8232 ECG sensor module [77], an ADS1115 ADC module [78], a microcontroller MEGA 2560 development board, and a personal computer. Fig. 3 shows the block diagram of the proposed circuit for ECG signal acquisition in the ECG/Real signal stage. This circuit extracts, filters, amplifies, and digitizes the ECG signal, which is acquired by the microcontroller using the I2C communication protocol between the microcontroller and the ADS1115. It is important to note that the purpose of this acquisition circuit is to monitor an ECG signal of a person, so its resources are sufficient to achieve this goal. The robustness of the proposed circuit against varying environmental conditions, such as changes in ambient noise, electrode-skin contact, and electromagnetic interference, has not been extensively validated. Recognizing these limitations not only enhances the transparency of this study but also provides a basis for future work aimed at optimizing both the algorithms and the acquisition hardware for broader real-world applications.

The expected ECG signal with the proposed hardware should consist of three main components: the differential ECG signal, the differential offset signal due to the electrodes, and the common-mode signal [79]. The differential ECG signal has a bandwidth ranging from 0.05 Hz to 150 Hz, with a peak-to-peak amplitude of approximately 1 mV, although it can reach up to 3 mV peak-to-peak. The interface between the skin and the electrode generates a low-frequency offset signal (±300 mV), which causes baseline wander [80]. The presence of BLW in the ECG signal can affect the interpretation of the data or, in the worst case, saturate the signal sequence. Finally, a common-mode component of up to 1.5 V can be generated due to the potential difference between the electrodes and ground. Potential artifacts affecting ECG signal quality include variations in skin-electrode contact, electromagnetic interference, and patient movement. These factors can introduce noise or distortions, requiring careful preprocessing and filtering. It is worth mentioning that the ECG signals were acquired using the mentioned equipment in a nursing practice laboratory at the Universidad Autónoma de Zacatecas, Jalpa Campus. The signals were obtained from a single male individual, 47 years old, weighing 73 kg, and with a height of 1.63 m.

Acquiring biopotentials presents a challenge in biomedical applications. Circuits must have certain characteristics, such as high Common-Mode Rejection Ratio (CMRR), high amplification gain, ease of construction, low power consumption, and low-cost electronic components. The baseline wander removal performance of the I-UFIR

filter, Savitzky-Golay (S-G) smoother, and MODWT wavelet is intended to be evaluated under controlled conditions. However, it is important to acknowledge potential limitations. The effectiveness of these algorithms can be sensitive to parameter tuning. For example, the selection of $l$ in the I-UFIR filter, the polynomial degree and window size in the S-G smoother, and the decomposition levels in MODWT, where suboptimal parameter choices may degrade performance.

## IV. Results and Discussion

In this section, the results of the proposed algorithms for approximating the BLW will be discussed, both for synthetic signals and real signals acquired in the laboratory. In the first stage, the hypothesis is tested that the horizons $N_{IU}$ and $N_{SG}$ of the Iterative UFIR (I-UFIR) and Savitzky-Golay (S-G) algorithms, respectively, provide an estimation of the BLW when set equal to the sampling frequency plus one. In the second stage, a statistical analysis of the results of the proposed algorithms with the acquired signals will be presented for comparison, since the reference BLW signal is not available to calculate the MSE.

### A. Algorithm Performance on Synthetic Signals

Based on the process detailed in Fig. 3, synthetic signals were generated with three different sampling frequencies 250, 360, and 500 Hz, adding several levels of noise by modifying the standard deviation $\sigma$ to 0.05, 0.1, 0.15, and 0.2. Referring to equation (4), the amplitude $V$ of the BLW is kept constant at 0.5 mV, the period of the sine wave $T$ is set to 10, the slope $m$ is equal to 0.01, and $\varphi$ is equal to 5. For this work, the polarization term $S$ was not considered, i.e., $S = 0$ mV, as in the second data set generated in [67].

In Fig. 4, an example is shown of how the synthetic measurement was generated for the estimation of the BLW using the proposed algorithms. In Fig. 4a, the synthetic ECG signal is displayed using the *ecgsyn* function [76]. For the signal shown in Fig. 4a, a sampling frequency of 250 Hz was used, with approximately 60 beats, no additive noise within the function, an average heart rate of 82, and a heart rate standard deviation of 1. Additionally, a low-frequency (LF) to high-frequency (HF) ratio of LF/HF = 0.5 and an internal sampling frequency of 250 Hz were used.

In Fig. 4a, the synthetic ECG signal is shown, along with the baseline wander signal, generated with equation (4) and the previously mentioned parameters, and a Gaussian noise with a mean of zero and a standard deviation of 0.05. In Fig. 4b, the oscillatory behavior of the BLW can be observed. Finally, in Fig. 4c, the results of the BLW estimation from the proposed algorithms are plotted, Wavelet with 9 and 10 decompositions, and I-UFIR and S-G with the horizon set equal to the sampling frequency plus one unit.

To estimate the optimal horizon $\widehat{N}_{opt}$ of the I-UFIR and S-G algorithms, the mean squared error must first be calculated as follows:

$$\epsilon(N) = E\{[b_k - \hat{x}_k(N)]^2\} \tag{15}$$

where $b_k$ is the BLW described in equation (4), and $\hat{x}_k$ is the BLW estimation using I-UFIR or S-G with different values of $N$. A polynomial approximation of degree six is then performed on $\epsilon$(N), so that $\hat{\epsilon}(N) = fit_6[\epsilon(N)]$, and $N_{opt}$ is calculated as:

$$\widehat{N}_{opt} = \left|\frac{\partial}{\partial N}(\hat{\epsilon}(N))\right| \tag{16}$$

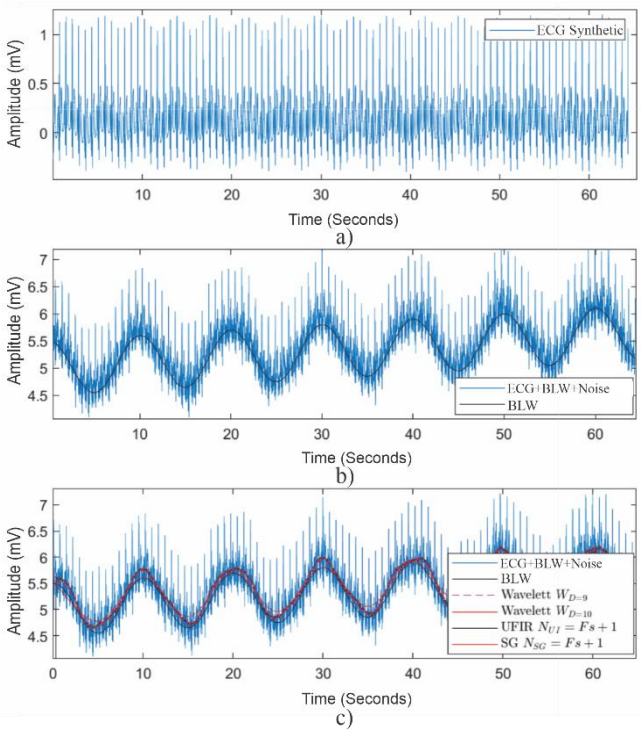


Fig. 4. ECG Signal Simulation for Baseline Wander Estimation Comparison: a) Synthetic Signal, b) Synthetic Signal with Baseline Wander and Gaussian Noise, c) Baseline Wander Estimation with Different Algorithms

A sixth-degree polynomial approximation was chosen because it provided the best fit based on the least squares $R^2$ metric, which was the most accurate in the previous example. This ensures a precise estimation of $N_{opt}$, minimizing fitting errors and improving the reliability of the I-UFIR and S-G algorithms, as illustrated in Fig. 5a and Fig. 5b. Fig. 5a and Fig. 5b show the process described above. In Fig. 5a, it can be seen how the error decreases as the horizon $N$ increases in both filters. In Fig. 5b, it is shown how a local minimum can be identified by taking the derivative in equation (16). The approach of setting the horizon $N$ of the I-UFIR or S-G filter to the sampling frequency plus one enables an effective approximation of the ECG baseline. This selection ensures that the window is large enough to average the PQRST complex, preventing the filter from tracking rapid fluctuations like the R peak while still capturing slow baseline variations. The additional unit ensures an odd window size, maintaining symmetry in the filtering process and enhancing stability and accuracy in baseline estimation.

For the implementation of the Wavelet algorithm, various decompositions and different families of orthonormal wavelets were used. However, for the synthetic signals, the best results were obtained using the "Symlets" family and 9 and 10 decompositions. The Symlets wavelets were chosen due to their near-symmetrical properties and improved time-frequency localization, which reduce signal distortion while preserving key features. Once the discrete wavelet transform

with maximal overlap was calculated, a multiresolution analysis was performed, so that the resulting signals were the BLW estimations.

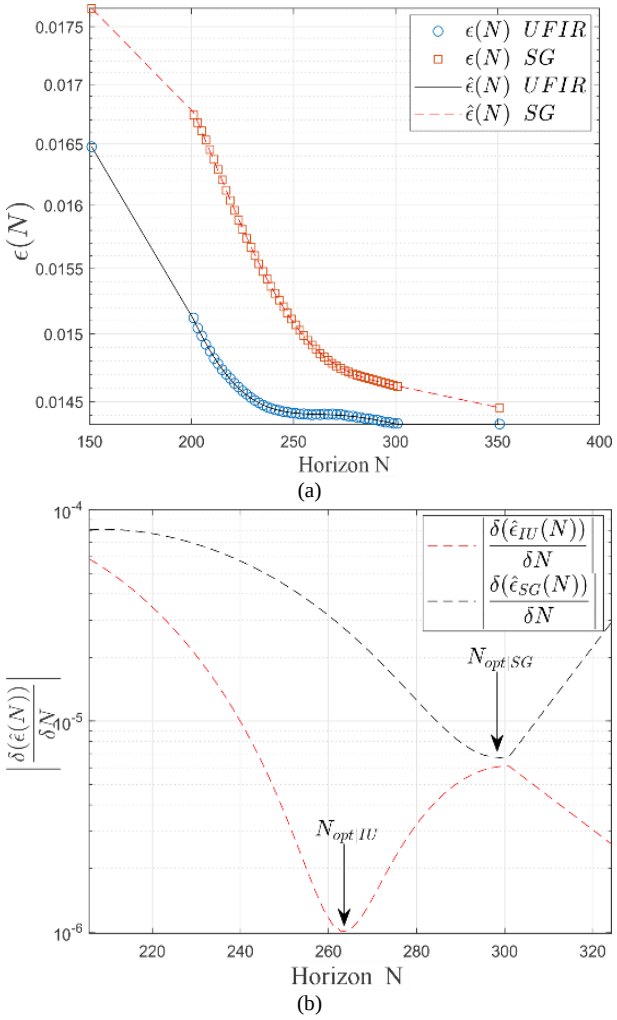


Fig. 5. Procedure for Calculating the Optimal Horizon Based on a Synthetic Signal Sampled at 250 Hz. a) Mean Squared Error and Curve Fitting with a 6th Degree Polynomial for the I-UFIR and S-G Algorithms, b) Absolute Value of the Partial Derivative of the Approximate Function for the I-UFIR and S-G Algorithms

Table I shows the results of the minimum squared error for the proposed techniques in this study, for signals generated with different sampling frequencies and varying noise simulation parameters. Here, it can be seen that the minimum error values are obtained using the Wavelet technique with 9 decompositions for Fs=250 and with 10 decompositions for Fs=360 Hz and Fs=500 Hz. The error results from the I-UFIR and S-G filters are similar, with differences on the order of $10^{-4}$. However, the minimum values in most cases are recorded by the S-G filter, with a horizon calculated using the relationship $N_{SG} = min\left|\sqrt{f_2}\right|$. It should be noted that the errors obtained by both filters show the same differences of $10^{-4}$ when the horizon is set equal to the sampling frequency plus one. It is also noticeable that, in most cases, when the optimal horizon is calculated, the S-G filter achieves a lower error than the I-UFIR filter. However, it is also important to highlight that the horizon size used by the S-G filter is always larger.

In Fig. 6, the difference in mean squared error results using different sampling frequencies and varying levels of noise added to the synthetic signals can be seen. In the graph of Fig. 6a, it can be observed that the technique using Wavelet with 9 decompositions achieves the lowest MSE for any noise level. This is followed by the I-UFIR and S-G techniques, using both horizon calculation methods, with an approximate difference of $2 \times 10^{-3}$. The algorithm with the highest error is Wavelet with 10 decompositions.

In Fig. 6b and Fig. 6c, the behavior of the proposed techniques is different. In the graph of Fig. 6b, the BLW estimation using Wavelet with 9 and 10 decompositions achieved the lowest MSE. The I-UFIR and S-G filters with the proposed horizons obtained similar errors, with an approximate difference of $\pm 5 \times 10^{-4}$. In Fig. 6c, the differences between Wavelet with 9 decompositions, I-UFIR, and S-G are smaller, highlighting the low error level of Wavelet with 10 decompositions. In this first stage, we can confirm that by calculating the baseline with a horizon of $N = Fs + 1$, I-UFIR and S-G algorithms provide an adequate estimation of the BLW.

TABLE I. RESULTS OF THE MINIMUM MSE FOR BASELINE WANDER ESTIMATION USING WAVELET TECHNIQUES WITH 9 AND 10 DECOMPOSITIONS, I-UFIR AND S-G

| Simulation Parameters | | Mean Square Error | | | | | |
|---|---|---|---|---|---|---|---|
| Sample Frequency | BLW | W9 | W10 | I-UFIR, $N_{IU} = F_s + 1$ | I-UFIR, $N_{IU} = min\left\|\sqrt{f_1}\right\|$ | SG, $N_{SG} = F_s + 1$ | SG $N_{SG} = min\left\|\sqrt{f_2}\right\|$ |
| Fs=250 | Bw=0.5,σ=0.05 | **0.012785** | 0.020634 | 0.014623 | 0.01440, N =263 | 0.014821 | 0.014551, N =299 |
| | Bw=0.5, σ =0.1 | **0.01257** | 0.020399 | 0.014506 | 0.01440, N =263 | 0.01471 | 0.01447, N =297 |
| | Bw=0.5, σ=0.15 | **0.012791** | 0.020708 | 0.015158 | 0.015139, N =267 | 0.015081 | 0.014553, N =313 |
| | Bw=0.5, σ =0.2 | **0.01244** | 0.02012 | 0.015012 | 0.014992, N =263 | 0.01553 | 0.014956, N =313 |
| | Bw=0.5, σ =0.5 | **0.01520** | 0.0223 | 0.01661 | 0.01609, N =289 | 0.01725 | 0.01650, N =325 |
| Fs=360 | Bw=0.5, σ =0.05 | 0.015239 | **0.0140** | 0.015868 | 0.015862, N =379 | 0.016234 | 0.015802, N =425 |
| | Bw=0.5, σ =0.1 | 0.015019 | **0.0140** | 0.015918 | 0.015915, N =375 | 0.016323 | 0.015553, N =429 |
| | Bw=0.5, σ =0.15 | 0.015350 | **0.01412** | 0.016043 | 0.01603, N =377 | 0.016416 | 0.01591, N =441 |
| | Bw=0.5, σ =0.2 | 0.015272 | **0.01412** | 0.016161 | 0.016149, N =377 | 0.016412 | 0.016071, N =435 |
| | Bw=0.5, σ =0.5 | 0.01569 | **0.01500** | 0.01670 | 0.016647, N =377 | 0.01753 | 0.016722, N =447 |
| Fs=500 | Bw=0.5, σ =0.05 | 0.01788 | **0.01595** | 0.01814 | 0.018226, N =525 | 0.018509 | 0.018056, N =595 |
| | Bw=0.5, σ =0.1 | 0.018010 | **0.016022** | 0.01826 | 0.018257, N =525 | 0.018676 | 0.018205, N =595 |
| | Bw=0.5, σ =0.15 | 0.0181 | **0.016000** | 0.018347 | 0.018337, N =527 | 0.018715 | 0.01828, N =593 |
| | Bw=0.5, σ =0.2 | 0.0181 | **0.0161** | 0.018453 | 0.018442, N =527 | 0.018823 | 0.01835, N =593 |
| | Bw=0.5, σ =0.5 | 0.01864 | **0.01626** | 0.01949 | 0.018902, N =529 | 0.01945 | 0.018854, N =593 |

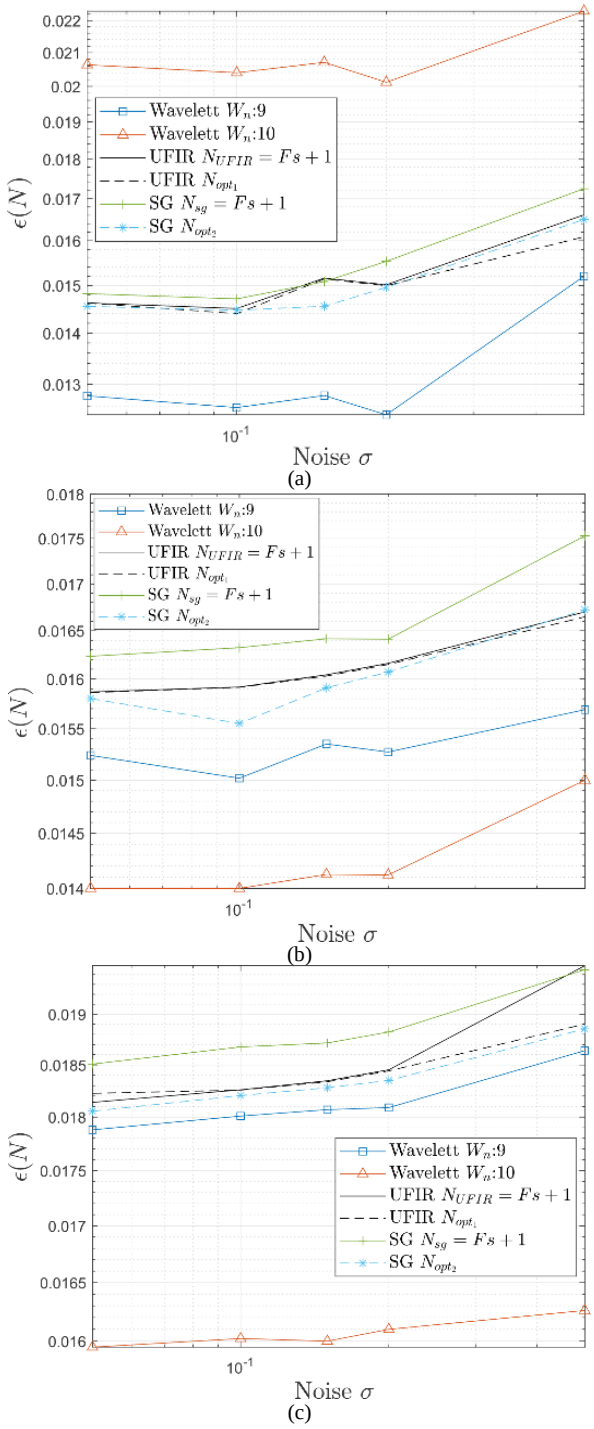


Fig. 6. Graphical Comparison of the Best Mean Squared Error Results at Different Noise Levels $\sigma$ for the Proposed Techniques for BLW Estimation. MSE for Different Sampling Frequencies: a) 250 Hz, b) 360 Hz, and c) 500 Hz

The Wavelet method achieved the lowest MSE in estimating baseline wander in ECG synthetic signals but at a higher computational cost. In contrast, the I-UFIR and S-G filters offer a trade-off between accuracy and efficiency, making them more suitable for real time applications. The choice of method depends on application requirements, where Wavelets are preferable for minimizing MSE when computational resources allow, while I-UFIR remains a competitive alternative for low-power or real-time scenarios.

These results can be supported based on Table II, which presents the results for the Root Mean Squared Error (RMSE) for the proposed techniques in this study, based on signals generated with different sampling frequencies and varying noise simulation parameters. Notably, the RMSE values closely mirror those of the MSE, reflecting a similar trend across different techniques. However, it is important to highlight the key distinction between these two metrics. While MSE provides a general measure of the squared differences between predicted and actual values, RMSE offers a more interpretable scale by taking the square root of the MSE, making it easier to assess the magnitude of the error in the same units as the original data. In this case, the lowest RMSE values are again achieved using the Wavelet technique with 9 decompositions for Fs=250 Hz, and with 10 decompositions for Fs=360 Hz and Fs=500 Hz.

### *B. ECG Extraction without External Converter A/D*

For the BLW estimation, an initial test was conducted without an external Analog-Digital (AD) converter, establishing a sampling frequency of 152 samples per second, using only the internal AD converter of the Arduino board. A sampling frequency of 152 was chosen because, after several tests with different sampling frequencies, this frequency best captured the main waves of an ECG as well as the desired behavior of BLW alteration. In Fig. 7a, the acquired ECG signal is shown, where BLW is present as the measurement exhibits intervals with changes in the mean and standard deviation. The same Fig. shows BLW estimations using the proposed techniques. For Wavelet with 9 and 10 decompositions, the decomposition that best fits the baseline was manually chosen. However, if a mean square error-based search with respect to the input signal is used, the results obtained with Wavelet are unsatisfactory. Each decomposition should be inspected to select the one that best approximates the baseline. Meanwhile, the I-UFIR and S-G filters calculated the baseline wander simply by tuning the horizon to the sampling frequency value, performing this task automatically.

TABLE II. RESULTS OF THE MINIMUM SQUARED ERROR FOR BASELINE WANDER ESTIMATION USING WAVELET TECHNIQUES WITH 9 AND 10 DECOMPOSITIONS, I-UFIR AND S-G

| Simulation Parameters | | Root Mean Square Error | | | | | |
|---|---|---|---|---|---|---|---|
| Sample Frequency | BLW | W9 | W10 | I-UFIR, $N_{IU} = F_s + 1$ | I-UFIR, $N_{IU} = min\lfloor\sqrt{f_1}\rfloor$ | SG, $N_{SG} = F_s + 1$ | SG $N_{SG} = min\lfloor\sqrt{f_2}\rfloor$ |
| Fs=250 | Bw=0.5, $\sigma$=0.05 | **0.113070** | 0.143645 | 0.120925 | 0.12, N =263 | 0.12174 | 0.120627, N =299 |
| | Bw=0.5, $\sigma$=0.1 | **0.112116** | 0.142825 | 0.120440 | 0.12, N =263 | 0.121284 | 0.1202913, N =297 |
| | Bw=0.5, $\sigma$=0.15 | **0.113097** | 0.143902 | 0.123117 | 0.123040, N =267 | 0.122804 | 0.120635, N =313 |
| | Bw=0.5, $\sigma$=0.2 | **0.111534** | 0.141844 | 0.122523 | 0.122441, N =263 | 0.124619 | 0.122294, N =313 |
| | Bw=0.5, $\sigma$=0.5 | **0.123288** | 0.149331 | 0.128879 | 0.126846, N =289 | 0.131339 | 0.128452, N =325 |
| Fs=360 | Bw=0.5, $\sigma$=0.05 | 0.123446 | **0.118321** | 0.125968 | 0.125944, N =379 | 0.127412 | 0.125706, N =425 |
| | Bw=0.5, $\sigma$=0.1 | 0.122552 | **0.118321** | 0.126166 | 0.126154, N =375 | 0.127761 | 0.124711, N =429 |
| | Bw=0.5, $\sigma$=0.15 | 0.123895 | **0.118827** | 0.126660 | 0.126609, N =377 | 0.128124 | 0.126134, N =441 |
| | Bw=0.5, $\sigma$=0.2 | 0.123579 | **0.118827** | 0.127125 | 0.127078, N =377 | 0.128109 | 0.126771, N =435 |
| | Bw=0.5, $\sigma$=0.5 | 0.125259 | **0.122474** | 0.12922 | 0.129023, N =377 | 0.132401 | 0.129313, N =447 |
| Fs=500 | Bw=0.5, $\sigma$=0.05 | 0.133716 | **0.126293** | 0.134684 | 0.135003, N =525 | 0.136047 | 0.134372, N =595 |
| | Bw=0.5, $\sigma$=0.1 | 0.134201 | **0.126578** | 0.135129 | 0.135118, N =525 | 0.136660 | 0.134925, N =595 |
| | Bw=0.5, $\sigma$=0.15 | 0.134536 | **0.126491** | 0.135451 | 0.135414, N =527 | 0.136802 | 0.13520, N =593 |
| | Bw=0.5, $\sigma$=0.2 | 0.134536 | **0.126885** | 0.135841 | 0.135801, N =527 | 0.137196 | 0.135462, N =593 |
| | Bw=0.5, $\sigma$=0.5 | 0.136528 | **0.127514** | 0.139606 | 0.137484, N =529 | 0.139463 | 0.137312, N =593 |

Fig. 7b, Fig. 7c, Fig. 7d, and Fig. 7e illustrate the resulting ECG signals after removing the estimated BLW with the techniques Wavelet $W_D = 9$, $W_D = 10$, I-UFIR, and S-G, respectively. Here, several observations can be made regarding the performance of each technique. The Wavelet $W_D$ =9 and $W_D$=10 decomposition offers a multi-resolution approach to baseline correction, its effectiveness strongly depends on selecting the appropriate decomposition level. As seen in Fig. 7b, and Fig. 7c, residual baseline drift persists, particularly after 20 seconds, suggesting that wavelet-based approaches may require adaptive thresholding or optimized decomposition selection methods to improve performance. Additionally, signal distortion may occur if an inappropriate level is chosen, leading to either excessive smoothing or insufficient BLW removal. On the contrary, the Iterative UFIR filter, see Fig. 7d, demonstrates superior BLW removal without requiring manual selection of parameters beyond tuning the horizon to the sampling frequency. This method effectively stabilizes the ECG baseline while preserving the morphology of the cardiac waveform, making it a robust alternative to wavelet decomposition. However, potential limitations include increased computational complexity compared to simpler filtering techniques. Similarly, the results of the SG filter, illustrated in Fig. 7e, also shows consistent baseline stabilization. Its polynomial smoothing capability helps maintain the integrity of high frequency components, reducing the likelihood of excessive smoothing observed in wavelet-based methods. However, SG filtering may be sensitive to window size selection, which could impact the overall balance between noise reduction and signal preservation.

In contrast to synthetic ECG signals where noise and baseline wander are typically well defined, real world signals introduce additional variability due to sensor noise, motion artifacts, and physiological variations. This highlights the limitations of static decomposition levels in wavelet filtering and emphasizes the advantage of I-UFIR and SG algorithms.

Since there is no reference baseline to determine the best technique for BLW estimation, a statistical comparison based on boxplots is proposed. It is worth remembering that a boxplot is a powerful tool that provides a concise visual summary of the error distribution of residuals of the model. The median line indicates the central tendency, if it is near zero, it suggests minimal systematic bias, whereas a deviation implies consistent over or underestimation. The interquartile range and whiskers reveal the spread of the residuals, with a narrow Interquartile Range (IQR) indicating low random error and a wide IQR, along with outliers, suggesting higher variability and occasional substantial deviations. Additionally, any skewness observed in the plot points to an uneven error distribution, potentially highlighting unaccounted factors or issues with the assumptions of the model.

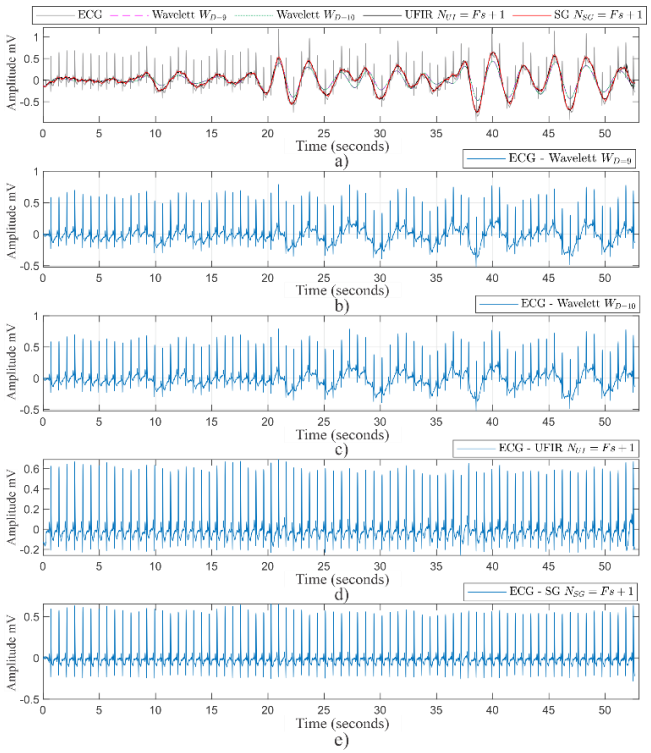


Fig. 7. a) Real ECG Signal Measurement without using the external converter and post-processing using various algorithms: b) Wavelet with 9 decompositions, c) Wavelet with 10 decompositions, d) I-UFIR, and e) SG

Fig. 8a, Fig. 8b, Fig. 8c, and Fig. 8d shows the boxplots of four different signals acquired at this stage. Generally, it can be deduced that the ECG measurements without BLW, calculated with Wavelet with 9 and 10 decompositions, show a broader range within $\pm 2.698\sigma$ across the four signals, meaning that approximately 99% of the information lies within this range. The I-UFIR and S-G algorithms exhibit a narrower range within $\pm 2.698\sigma$. However, only in the first signal does the I-UFIR filter present lower variation. In Fig. 8b, Fig. 8c, and Fig. 8d, Savitzky-Golay shows the most stable behavior. In addition to range and variability, the box plots further explain the distributional characteristics of the residuals. Notably, the median values for both the I-UFIR and S-G filters remain centered near zero across most signals, indicating that these methods effectively minimize systematic bias. Slight asymmetries in some plots suggest the presence of minor residual systematic errors that may warrant further investigation. Moreover, the fewer extreme outliers observed with the I-UFIR and S-G filters reinforce their robustness and consistent performance, underscoring its potential to reliably preserve key ECG morphological features across diverse signal conditions.

### *C. ECG Extraction with External Converter A/D*

For this stage, it was proposed to use the ADS1115 A/D converter to establish a more common sampling frequency for ECG signal acquisition. In this case, the A/D converter was tuned to collect data at 250 samples per second. From Fig. 9a to Fig. 9d aims to show the processing of signals acquired with the external A/D converter and the BLW line estimation. First, in Fig. 9a, the real ECG signal is shown, where the wavy movement of the BLW signal accompanying the ECG signal. In Fig. 9b, Fig. 9c, and Fig. 9d, the ECG signal is shown, where the BLW signal was removed using the Wavelet filter with 9 decompositions, and I-UFIR and S-G filters with the horizon set to the sampling frequency plus one, respectively.

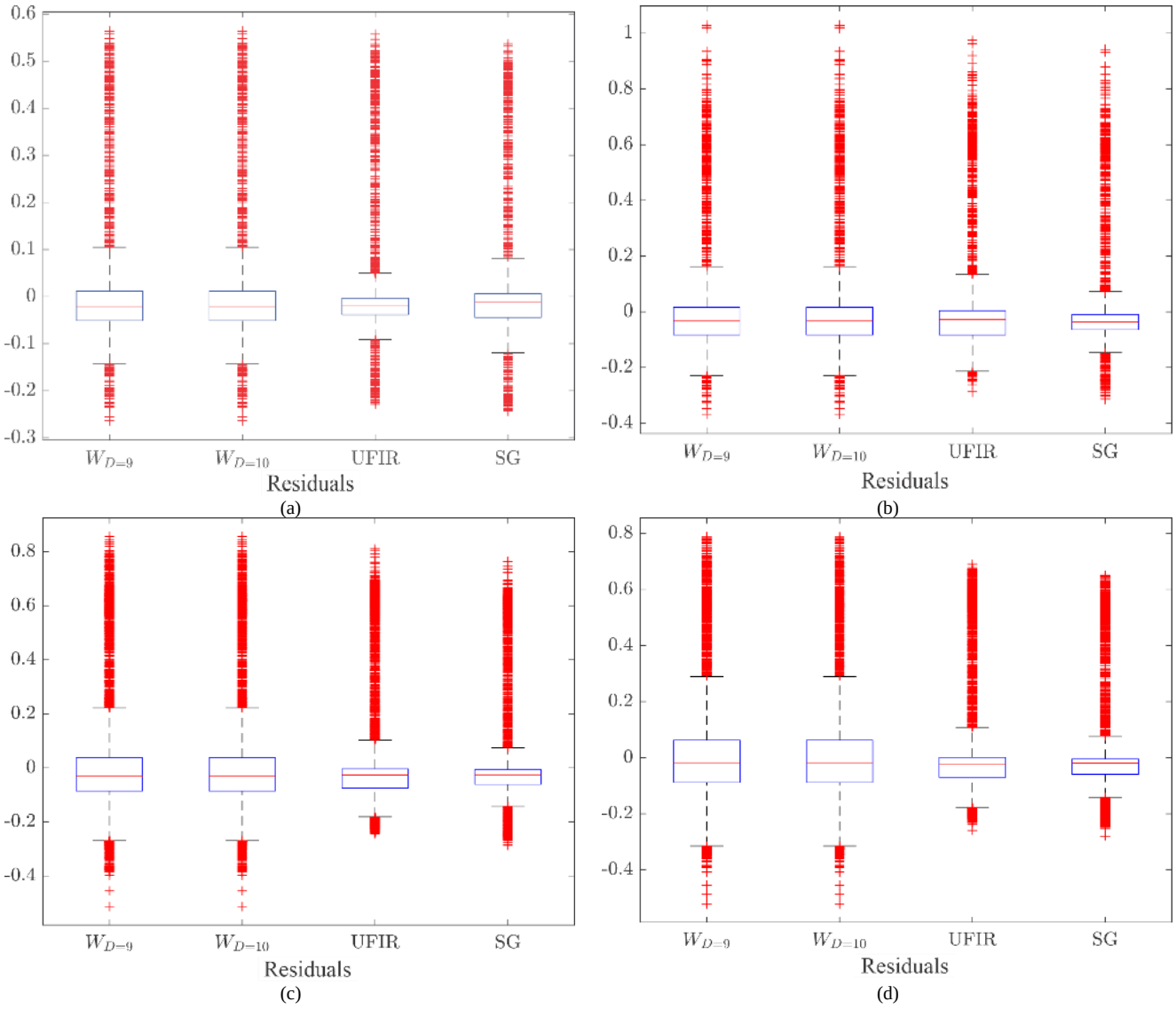


Fig. 8. Boxplot of real ECG measurements without BLW and without using an external A/D converter

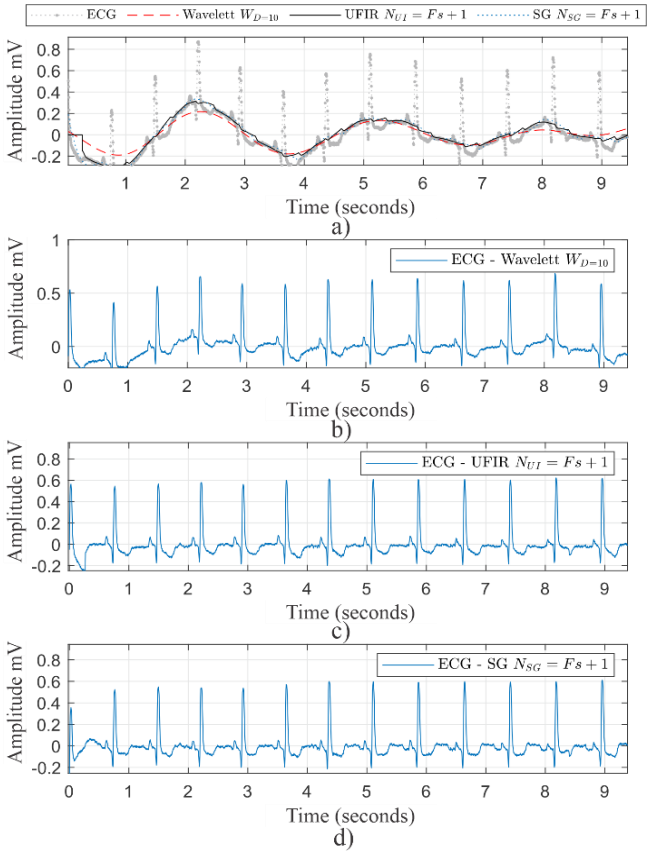


Fig. 9. Analysis of signals extracted with the ADS1115 A/D converter: a) Real ECG signal, b), c), and d) signals without BLW using the Wavelet, I-UFIR, and S-G filters, respectively

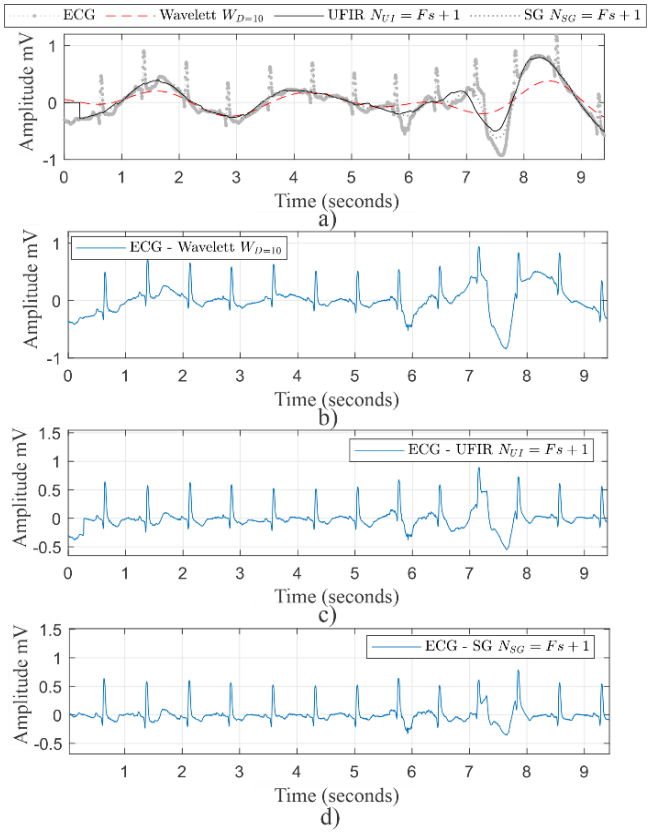


Fig. 10. Analysis of signals extracted with the ADS1115 A/D converter: a) Real ECG signal, b), c), and d) signals without BLW using the Wavelet, I-UFIR, and S-G filters, respectively

The second real ECG signal recorded using the external A/D converter is shown in Fig. 10a. Like the first signal, a wavy behavior is observed, but with higher amplitudes, along with abrupt changes in the signal. In Fig. 10b, Fig. 10c, and Fig. 10d, the ECG signals are shown once the BLW line was removed using the Wavelet filter with 9 decompositions, and the I-UFIR and S-G filters with the horizon set to the sampling frequency plus one, respectively. When closely examining the behavior of the acquired signal and the processed measurements during the 6 to 8-second interval, an abrupt change in the signal is noted, and the S-G technique is the one that stabilizes the signal to this change during this period. In contrast, the Wavelet filter with 9 decompositions, despite manually selecting the measurement that best fit the BLW, still preserves part of this behavior.

As mentioned earlier, since real signals lack a BLW reference to calculate the MSE, it is necessary to analyze the real ECG results recorded using an A/D converter through the boxplot tool. Fig. 11a, Fig. 11b, and Fig. 11c shows the boxplots of three recorded signals after the BLW signal was removed using the proposed filters. In Fig. 11a, it can be observed that the BLW estimation with the I-UFIR filter provides a signal with a narrower $\pm 2.698\sigma$ range. However, the result using the SG filter shows fewer outliers in the negative part of the ECG signal than the UFIR filter. Meanwhile, the result using Wavelet with 9 decompositions has the widest information distribution range.

For the real ECG signal 2 in Fig. 11b, the boxplots for the I-UFIR and S-G filters show similar results, with an upper limit difference of $\pm 2.698\sigma$ at $8.25 \times 10^{-3}$ and a lower limit difference of $9 \times 10^{-5}$. In contrast, the results using Wavelet, which accumulates 99% of the information over a wider interval than the previous filters, especially when using 9 decompositions. Finally, in a third test, the solution using the SG filter appears to have greater stability compared to the other techniques. This statement is based on the narrower whiskers compared to other techniques and the median being close to zero at -0.015869. In Fig. 11c, the third box plot further highlights the differences in variability and stability among the filtering methods. The Wavelet decomposition with 9 and 10 levels exhibits wider whiskers than the I-UFIR and S-G filters, indicating a higher spread of residuals. Notably, the Wavelet with 9 decompositions shows fewer outliers, likely due to its broader whiskers, which include more data within the interquartile range. In contrast, both the I-UFIR and S-G filters maintain narrower whiskers, reinforcing their ability to reduce variations while keeping the median centered near zero. Finally, in this third test, the S-G filter demonstrates the most stable performance, further confirming its robustness in preserving ECG signal morphology while minimizing baseline wander. The presence of outliers in the box plots of Fig. 8 and Fig. 11 can be attributed to several factors, including transient artifacts in the ECG signals, residual baseline wander that was not fully removed, and variations in signal acquisition conditions such as electrode contact instability or motion artifacts. In the case of Wavelet decomposition, wider whiskers suggest a greater spread of residuals, which may contribute to fewer detected

outliers, whereas the narrower whiskers in I-UFIR and S-G indicate more consistent filtering but may still leave some extreme residuals. These outliers could affect the overall performance by slightly increasing error metrics like MSE and RMSE, but their impact is localized rather than systematic.

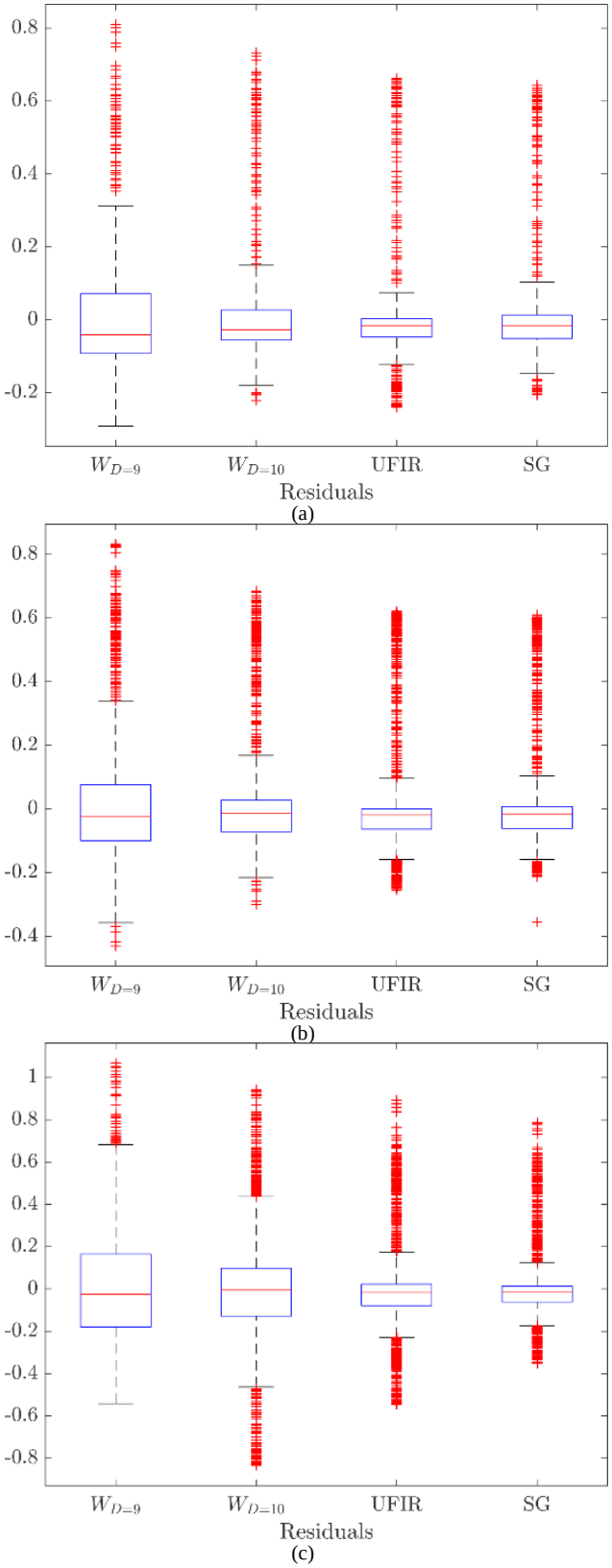


Fig. 11. Boxplot of real ECG measurements without BLW and using an external converter A/D

The previous results suggest that effective baseline wander removal has significant clinical implications, as preserving key ECG morphological features is essential for accurately diagnosing conditions like myocardial ischemia and arrhythmias. By minimizing distortions that can mask these critical features, the algorithms evaluated in this study have the potential to enhance automated ECG analysis and improve diagnostic reliability. Although technical metrics like MSE, RMSE, and boxplot provide quantitative and qualitative performance assessments, the ability of methods such as I-UFIR, Savitzky-Golay, and Wavelet transform to maintain ECG integrity directly translates into better patient care through more precise interpretation and reduced misdiagnoses. Ultimately, these improvements could support clinical decisions by reducing false positives and negatives, thereby facilitating timely and appropriate treatment interventions. While the study focuses on baseline wander removal, real world challenges such as electrode-skin contact variability, electromagnetic interference, and patient movement can introduce additional noise that affects ECG signal quality. These factors may impact the performance of the proposed algorithms by introducing transient artifacts or distortions that are not purely baseline wander, potentially reducing filtering effectiveness. Future work could explore adaptive filtering techniques or hybrid approaches that integrate motion artifact reduction to enhance robustness in practical settings. Additionally, evaluating the algorithms on ECG data collected under varying real world conditions would provide further insight into their reliability and applicability in clinical and ambulatory environments.

## V. CONCLUSIONS

This work highlighted the inherent presence of baseline wander in ECG signals and the importance of its estimation and removal to obtain more stable measurements for detecting future parameters. To achieve this, the I-UFIR, S-G, and Wavelet filters were used, with the latter being one of the most widely used techniques in the literature. The comparison of these algorithms was conducted in two scenarios, one by generating synthetic signals to provide a reference BLW. In this test, it was observed that the Wavelet technique, with 9 and 10 decompositions, was the most suitable for estimating the BLW based on results from the minimum Mean Square Error (MSE) and Root Mean Square Error (RMSE). The results demonstrated that for Fs = 250 Hz and noise with $\sigma = 0.5$, Wavelet decomposition with 9 levels achieved the lowest error, with MSE = 0.01520 and RMSE = 0.123288, making it the most suitable method for these synthetic signals. For Fs = 360 Hz and Fs = 500 Hz with noise with =0.5, wavelet decomposition with 10 levels also achieved the lowest error, with MSE = 0.01500 and RMSE = 0.01626 for Fs = 360 Hz, and MSE = 0.01500 and RMSE = 0.127514 for Fs = 500 Hz, making it the most suitable method under these conditions. However, the I-UFIR and S-G proposals, using two different horizons, showed no significant differences in MSE compared to those obtained by Wavelet.

In contrast, in a second experimental stage, where a basic and low-cost ECG signal acquisition system was proposed, this work demonstrated that, while the Wavelet technique excelled in synthetic signals with 9 and 10 decompositions,

the I-UFIR and S-G filters were more effective for BLW estimation in real world ECG scenarios. This advantage is potentially due to their simplicity, lower computational requirements, and robustness under noise, making them better suited for practical applications in low-cost hardware. These algorithms successfully reduced the impact of BLW in the acquired ECG signals, as verified by a statistical analysis with boxplots. Although both I-UFIR and S-G filters were effective, the slight advantage of the S-G filter, as evidenced by boxplot analysis, may be attributed to its better handling of specific frequency components in the ECG signal, resulting in slightly better performance than I-UFIR. In both experimental stages, the disadvantage of calculating the optimal horizon for I-UFIR and S-G was mitigated by matching this parameter. The approach based on setting the horizon to the sampling frequency plus one guarantees that the window is sufficiently large to average the entire PQRST complex. Consequently, the filter avoids tracking rapid fluctuations, such as the R peak, while still capturing slow baseline drifts.

Finally, it is worth mentioning that the effective implementation of I-UFIR and S-G filters in low-cost ECG acquisition systems emphasizes their potential for improving the accuracy and stability of wearable health monitoring devices. This conclusion is supported by the narrower whiskers observed in these techniques, along with the median value, which is closer to zero in most cases, indicating enhanced performance compared to other methods. Given their computational efficiency and adaptability to resource-constrained hardware, these techniques could play a key role in advancing real-time ECG signal processing for remote patient monitoring and medical diagnostics. However, this study has certain limitations that should be considered. First, the evaluation of BLW removal was conducted on ECG signals obtained from a single individual under controlled conditions, which may limit the generalizability of the findings to a broader population or different ECG recording environments. The hardware setup used for real ECG acquisition, while designed to be low-cost and accessible, may introduce specific artifacts or limitations that could influence the performance of the filtering techniques. Future work could focus on applying these methods to different biomedical signals or examining their combination with machine learning models to enhance ECG signal quality and facilitate automated diagnosis. Also, it would be interesting to explore incorporating stochastic models or adaptive techniques to better account for the real-world variations in ECG signals.

## REFERENCES


[1] World Health Organization (WHO), Noncommunicable diseases, *World Health Organization (WHO)*, 2023,https://www.who.int/news-room/fact-sheets/detail/noncommunicable-diseases.

[2] M. Y. Henein, S. Vancheri, G. Longo, and F. Vancheri, "The role of inflammation in cardiovascular disease," *International Journal of Molecular Sciences*, vol. 23, no. 21, p. 12906, 2022, doi: 10.3390/ijms232112906.

[3] J. Ferlay, M. Colombet, I. Soerjomataram, D. M. Parkin, M. Piñeros, A. Znaor, and F. Bray, "Cancer statistics for the year 2020: An overview," *International Journal of Cancer*, vol. 149, no. 4, pp. 778-789, 2021, doi: 10.1002/ijc.33588.

[4] G. Viegi, S. Maio, S. Fasola, and S. Baldacci, "Global burden of chronic respiratory diseases," *Journal of Aerosol Medicine and Pulmonary Drug Delivery*, vol. 33, no. 4, pp. 171-177, 2020, doi: 10.1089/jamp.2019.1576.

[5] J. B. Cole, and J. C. Florez, "Genetics of diabetes mellitus and diabetes complications," *Nature Reviews Nephrology*, vol. 16, no. 7, pp. 377-390, 2020, doi: 10.1038/s41581-020-0278-5.

[6] H. T. Cheng, X. Xu, P. S. Lim, and K. Y. Hung, "Worldwide epidemiology of diabetes-related end-stage renal disease, 2000–2015", *Diabetes Care*, vol. 44, no. 1, pp. 89-97, 2021, doi: 10.2337/dc20-1913.

[7] World Health Organization (WHO), *Cardiovascular diseases*. World Health Organization (WHO), 2024, https://www.who.int/health-topics/cardiovascular-diseases#tab=tab_1.

[8] G. Lippi and F. Sanchis-Gomar, "An estimation of the worldwide epidemiologic burden of physical inactivity-related ischemic heart disease," *Cardiovascular Drugs and Therapy*, vol. 34, pp. 133-137, 2020, doi: 10.1007/s10557-019-06926-5.

[9] L. B. Goldstein, "Introduction for focused updates in cerebrovascular disease," *Stroke*, vol. 51, no. 3, pp. 708-710, 2020, doi: 10.1161/STROKEAHA.119.024159.

[10] S. H. Ghamari *et al*., "Rheumatic heart disease is a neglected disease relative to its burden worldwide: findings from global burden of disease 2019," *Journal of the American Heart Association*, vol. 11, no. 13, p. e025284, 2022, doi: 10.1161/JAHA.122.025284.

[11] C. Lai, S. Zhou, and N. A. Trayanova, "Optimal ECG-lead selection increases generalizability of deep learning on ECG abnormality classification," *Philosophical Transactions of the Royal society A*, vol. 379, no. 2212, p. 20200258, 2021, doi: 10.1098/rsta.2020.0258.

[12] H. Li and P. Boulanger, "A survey of heart anomaly detection using ambulatory electrocardiogram (ECG)," *Sensors*, vol. 20, no. 5, p. 1461, 2020, doi:10.3390/s20051461.

[13] K. Nezamabadi, N. Sardaripour, B. Haghi, and M. Forouzanfar, "Unsupervised ECG analysis: A review", *IEEE Reviews in Biomedical Engineering*, vol. 16, pp. 208-224, 2022, doi: 10.1109/RBME.2022.3154893.

[14] H. De Carvalho *et al*., "Electrocardiographic abnormalities in COVID-19 patients visiting the emergency department: a multicenter retrospective study," *BMC Emergency Medicine*, vol. 21, pp. 1-7, 2021, doi: 10.1186/s12873-021-00539-8.

[15] A. Pal, R. Srivastva, and Y. N. Singh, "CardioNet: An efficient ECG arrhythmia classification system using transfer learning," *Big Data Research*, vol. 26, p. 100271, 2021, doi: 10.1016/j.bdr.2021.100271.

[16] P. Madona, R. I. Basti, and M. M. Zain, "PQRST wave detection on ECG signals," *Gaceta sanitaria*, vol. 35, pp. S364-S369, 2021, doi: 10.1016/j.gaceta.2021.10.052.

[17] S. Chatterjee, R. S. Thakur, R. N. Yadav, L. Gupta, and D. K. Raghuvanshi, "Review of noise removal techniques in ECG signals," *IET Signal Processing*, vol. 14, no. 9, pp. 569-590, 2020, doi: 10.1049/iet-spr.2020.0104.

[18] H. Y. Mir and O. Singh, "ECG denoising and feature extraction techniques–a review," *Journal of medical engineering & technology*, vol. 45, no. 8, pp. 672-684, 2021, doi: 10.1080/03091902.2021.1955032.

[19] J. Zhang, Y. Guo, X. Dong, T. Wang, J. Wang, X. Ma, and H. Wang, "Opportunities and challenges of noise interference suppression algorithms for dynamic ECG signals in wearable devices: A review," *Measurement*, vol. 259, p. 117067, 2025, doi: 10.1016/j.measurement.2025.117067.

[20] M. R. Alla, and C. Nayak, "A robust ECG signal enhancement technique through optimally designed adaptive filters," *Biomedical Signal Processing and Control*, vol. 95, p. 106434, 2024, doi: 10.1016/j.bspc.2024.106434.

[21] A. H. Kashou *et al*., "ECG interpretation proficiency of healthcare professionals," *Current Problems in Cardiology*, vol. 48, no. 10, 2023, doi: 10.1016/j.cpcardiol.2023.101924.

[22] J. Frampton, A. R. Ortengren, and E. P. Zeitler, "Arrhythmias after acute myocardial infarction," *The Yale journal of biology and medicine*, vol. 96, no. 1, p. 83, 2023, doi: 10.59249/LSWK8578.

[23] X. Xu, Z. Wang, J. Yang, X. Fan, and Y. Yang, "Burden of cardiac arrhythmias in patients with acute myocardial infarction and their impact on hospitalization outcomes: insights from China acute myocardial infarction (CAMI) registry," *BMC Cardiovascular*

*Disorders*, vol. 24, no. 1, p. 218, 2024, doi: 10.1186/s12872-024-03889-w.

[24] A. Menditto, L. Mancinelli, and R. Antonicelli, "Autonomic nervous system and cardiac arrhythmias," *In Autonomic Disorders in Clinical Practice*, pp. 43-64, 2023, doi: 10.1007/978-3-031-43036-7_4.

[25] T. Neycheva, D. Dobrev, and V. Krasteva, "Common-mode driven synchronous filtering of the powerline interference in ECG," *Applied Sciences*, vol. 12, no. 22, pp. 1-29, 2022, doi: 10.3390/app122211328.

[26] J. Shen, X. Li, Y. Wang, Y. Li, J. Bian, X. Zhu, X. He, and J. Li, "Anti-motion Interference Electrocardiograph Monitoring System-A Review," *IEEE Sensors Journal*, vol. 24, no. 10, pp. 15727-15747, 2024, doi: 10.1109/JSEN.2024.3383872.

[27] A. Singhal, P. Singh, B. Fatimah, and R. B. Pachori, "An efficient removal of power-line interference and baseline wander from ECG signals by employing Fourier decomposition technique," *Biomedical Signal Processing and Control*, vol. 57, p. 101741, 2020, doi: 10.1016/j.bspc.2019.101741.

[28] S. Boda, M. Mahadevappa, and P. K. Dutta, "A hybrid method for removal of power line interference and baseline wander in ECG signals using EMD and EWT," *Biomedical Signal Processing and Control*, vol. 67, p. 102466, 2021, doi: 10.1016/j.bspc.2021.102466.

[29] X. Wan, H. Wu, F. Qiao, F. Li, Y. Li, Y. Yan, and J. Wei, "Electrocardiogram baseline wander suppression based on the combination of morphological and wavelet transformation-based filtering", *Computational and Mathematical Methods in Medicine*, vol. 2019, pp. 1-7, 2019, doi: 10.1155/2019/7196156.

[30] M. Khalili, H. GholamHosseini, A. Lowe, and M. M. Y. Kuo, "Motion artifacts in capacitive ECG monitoring systems: a review of existing models and reduction techniques," *Medical & Biological Engineering & Computing*, vol. 62, pp. 3599-3622, 2024, doi: 10.1007/s11517-024-03165-1.

[31] M. K. Islam, A. Rastegarnia, and S. Sanei, "Signal artifacts and techniques for artifacts and noise removal," *Signal Processing Techniques for Computational Health Informatics*, pp. 23-79, 2021, doi:10.1007/978-3-030-54932-9_2.

[32] L. Littmann, "Electrocardiographic artifact," *Journal of Electrocardiology*, vol. 64, pp. 23-29, 2021, doi: 10.1016/j.jelectrocard.2020.11.006.

[33] S. Ozaydin and I. Ahmad, "Comparative Performance Analysis of Filtering Methods for Removing Baseline Wander Noise from an ECG Signal," *Fluctuation and Noise Letters*, vol. 23, no. 4, 2024, doi: 10.1142/S0219477524500469.

[34] F. P. Romero, D. C. Piñol, and C. R. V. Seisdedos, "DeepFilter: An ECG baseline wander removal filter using deep learning techniques," *Biomedical Signal Processing and Control*, vol. 70, pp. 1-122, 2021, doi: 10.48550/arXiv.2101.03423.

[35] H. Li, G. Ditzler, J. Roveda, and A. Li, "Descod-ecg: Deep score-based diffusion model for ecg baseline wander and noise removal," *IEEE Journal of Biomedical and Health Informatics*, vol. 28, no. 9, pp. 5081-5091, 2023, doi: 10.1109/JBHI.2023.3237712.

[36] L. Yao and Z. Pan, "A new method based CEEMDAN for removal of baseline wander and powerline interference in ECG signals," *Optik*, vol. 223, p. 165566, 2020, doi: 10.1016/j.ijleo.2020.165566.

[37] R. Kher, "Signal Processing Techniques for Removing Noise from ECG Signals", *Journal of Biomedical Engineering and Research*, vol. 3, pp. 1-9, 2019, doi: 10.17303/jber.2019.3.101.

[38] A. Pashko, I. Krak, O. Stelia, and W. Wojcik, "Baseline wander correction of the electrocardiogram signals for effective preprocessing," *Lecture Notes in Computational Intelligence and Communications Technologies*, vol. 77, pp. 507-518, 2022, doi: 10.1007/978-3-030-82014-5_34.

[39] J. Rahul, and M. Sora, "An efficient algorithm for the removal of motion artifacts in wearable ECG technology," *Iran J Comput Sci*., vol. 8, pp. 69–78, 2025. doi: 10.1007/s42044-024-00208-6.

[40] A. A. Fedotov, "An adaptive method for correction of the ECG signal baseline drift using multiresolution wavelet transforms," *Biomedical Engineering*, vol. 55, no. 6, pp. 420-424, 2022, doi: 10.1007/s10527-022-10149-8.

[41] H. B. Hwang, H. Kwon, B. Chung, J. Lee, and I. Y. Kim, "ECG authentication based on non-linear normalization under various physiological conditions," *Sensors*, vol. 21, no. 21, p. 6966, 2021, doi: 10.3390/s21216966.

[42] F. P. Romero, L. V. Romaguera, C. F. F. Costa-Filho, M. G. Fernandes, J. Evangelista, and C. R. V. Seisdedos, "Baseline wander removal methods for ECG signals: A comparative study," *Revista Cubana de Ciencias Informáticas*, vol. 14, no. 1, pp. 1-19, 2019, doi: 10.48550/arXiv.1807.11359.

[43] N. E. Menaceur, S. Kouah, and M. Derdour, "Adaptive Filtering Strategies for ECG Signal Enhancement: A Comparative Study," *6th International Conference on Pattern Analysis and Intelligent Systems (PAIS)*, pp. 1-6, 2024 doi: 10.1109/PAIS62114.2024.10541144.

[44] M. R. Lakehal, and Y. Ferdi, "Baseline wander and power line interference removal from physiological signals using fractional notch filter optimized through genetic algorithm," *Arabian Journal for Science and Engineering*, vol. 49, no. 12, pp. 16647-16667, 2024, doi: 10.1007/s13369-024-09145-9.

[45] P. Madan, V. Singh, D. P. Singh, M. Diwakar, and A. Kishor, "Denoising of ECG signals using weighted stationary wavelet total variation," *Biomedical Signal Processing and Control*, vol. 73, p. 103478, 2022, doi: 10.1016/j.bspc.2021.103478.

[46] G. B. Moody and R. G. Mark, "The impact of the MIT-BIH Arrhythmia Database," *IEEE Engineering in Medicine and Biology Magazine*, vol. 20, no. 3, 2001, doi: 10.1109/51.932724.

[47] A. L. Goldberger *et al*., "PhysioBank, PhysioToolkit, and PhysioNet: Components of a New Research Resource for Complex Physiologic Signals," *Circulation*, vol. 101, no. 23, pp. 215-220, 2000, doi: 10.1161/01.CIR.101.23.e215.

[48] M. J. S. M. A. Maraikkayar *et al*., "Novel digital filter design for noise removal in fetal ECG signals," *The Open Biomedical Engineering Journal*, vol. 17, no.1, pp. 1-8, 2023, doi: 10.2174/18741207-v16-e221227-2022-HT27-3589-8.

[49] M. Aqil, A. Jbari, and A. Bourouhou, "Comparison of ECG baseline wander removal techniques and improvement based on moving average of wavelet approximation coefficients," *International Journal Bioautomation*, vol. 25, no. 2, pp. 183-204, 2021, doi: 10.7546/ijba.2021.25.2.000770.

[50] R. M. Raj, V. Rajesh, S. Saravanan, M. S. P. Balaji, and V. Elamaran, "Baseline wandering noise removal using high-speed IIR filters with an FPGA implementation," *Microelectronic Devices, Circuits and Systems: Second International Conference*, ICMDCS 2021, vol. 1392, pp. 55-65, 2021, doi: 10.1007/978-981-16-5048-2_5.

[51] R. Chitra and E. Priya, "Digital filter implementation for removal of baseline wander in ECG signals," *In International Conference on Automation, Signal Processing, Instrumentation and Control, Singapore: Springer Nature Singapore*, pp. 2711-2718, 2020, doi: 10.1007/978-981-15-8221-9_254.

[52] I. Houamed, L. Saidi, and F. Srairi, "ECG signal denoising by fractional wavelet transform thresholding," *Research on Biomedical Engineering*, vol. 36, pp. 349-360, 2020, doi: 10.1007/s42600-020-00075-7.

[53] C. C. Chen, and F. R. Tsui, "Comparing different wavelet transforms on removing electrocardiogram baseline wanders and special trends," *BMC medical informatics and decision making*, vol. 20, pp. 1-10, 2020, doi: 10.1186/s12911-020-01349-x.

[54] S. A. Malik, S. A. Parah, and B. A. Malik, "Power line noise and baseline wander removal from ECG signals using empirical mode decomposition and lifting wavelet transform technique," *Health and Technology*, vol. 12, no. 4, pp. 745-756, 2022, doi:10.1007/s12553-022-00662-x.

[55] T. Tearwattanarattikal and A. Lek-uthai, "Comparison of baseline wander correction methods for handheld ECG with motion artefacts," *In 2022 37th International Technical Conference on Circuits/Systems, Computers and Communications (ITC-CSCC)*, pp. 1-4, 2022, doi: 10.1109/ITC-CSCC55581.2022.9894859.

[56] B. R. Manju and M. R. Sneha, "ECG denoising using Wiener filter and Kalman filter", in *Third International Conference on Computing and Network Communications (CoCoNet'19)*, pp. 273-281, 2019, doi: 10.1016/j.procs.2020.04.029.

[57] B. M. Manjula, R. Vivek, R. Nishant, N. S. Raja, M. Z. HN, and M. A. Goutham, "ECG denoising using multiple approaches," 2023 *International Conference on Data Science and Network Security (ICDSNS)*, pp. 1-6, 2023, doi: 10.1109/ICDSNS58469.2023.10245187.

[58] S. Tahir, M. M. Raja, N. Razzaq, A. Mirza, W. Z. Khan, S. W. Kim, and Y. B. Zikria, "Extended Kalman filter-based power line interference canceller for electrocardiogram signal," *Big Data*, vol. 10, no. 1, pp. 34-53, 2022, doi: 10.1089/big.2021.0043.

[59] A. K. Roonizi and R. Sassi, "Smoothing filter design: a general framework," *Biomedical Signal Processing and Control*, vol. 85, p. 104952, 2023, doi: 10.1016/j.bspc.2023.104952.

[60] V. Murugan and D. Panigrahy, "Optimized adaptive filter for powerline interference cancellation in electrocardiogram signal using a modified lightning search algorithm," *Circuits, Systems, and Signal Processing*, vol. 43, no. 10, pp. 6510-6536, 2024, doi:10.1007/s00034-024-02766-3.

[61] N. D. Jahromi and H. D. Jahromi, "An investigation on the performance of infinite impulse response filters in denoising electrocardiogram signals," *Transactions on Machine Intelligence*, vol. 6, no. 1, pp. 10-15, 2023, doi:10.47176/TMI.2023.10.

[62] S. Basu and S. Mamud, "Comparative study on the effect of order and cut off frequency of Butterworth low pass filter for removal of noise in ECG signal," *In 2020 IEEE 1st International Conference for Convergence in Engineering (ICCE)*, pp. 156-160, 2020, doi:10.1109/ICCE50343.2020.9290646.

[63] Y. S. Shmaliy, "Unbiased FIR filtering of discrete-time polynomial state-space models," *IEEE Transactions on Signal Processing*, vol. 57, no. 4, pp. 1241-1249, 2009, doi: 10.1109/TSP.2008.2010640.

[64] Y. S. Shmaliy and S. Zhao, "Optimal and robust state estimation: Finite Impulse Response (FIR) and Kalman approaches," *John Wiley & Sons*, 2022, doi:10.1002/9781119863106.

[65] C. Lastre-Domínguez, J. Muñoz-Minjares, E. Pérez-Campos, and Y. Shmaliy, "Denoising and time-frequency features extraction of ECG signals using iterative unbiased FIR algorithm," *In International Conference on Computing, Control and Industrial Engineering, Singapore: Springer Nature Singapore*, pp. 308-316, 2024, doi:10.1007/978-981-97-6937-7_37.

[66] J. U. Munoz-Minjares, M. Lopez-Ramirez, M. Vazquez-Olguin, C. Lastre-Dominguez, and Y. S. Shmaliy, "Outliers detection for accurate HRV-seizure baseline estimation using modern numerical algorithms," *Biomedical Signal Processing and Control*, vol. 67, p. 102553, 2021, doi: 10.1016/j.bspc.2021.102553.

[67] M. Khosravy, N. Gupta, N. Patel, T. Senjyu, and C. A. Duque, "Particle swarm optimization of morphological filters for electrocardiogram baseline drift estimation," *Applied Nature-Inspired Computing: Algorithms and Case Studies*, pp. 1-21, 2020, doi: 10.1007/978-981-13-9263-4_1.

[68] A. Osadchiy, A. Kamenev, V. Saharov, and S. Chernyi, "Signal processing algorithm based on discrete wavelet transform," *Designs*, vol. 5, no. 3, p. 41, 2021, doi:10.3390/designs5030041.

[69] M. A. Basarab, "The new wavelet-like Allan variance based on the atomic function," In *2021 Photonics & Electromagnetics Research Symposium (PIERS)*, pp. 2870-2877, 2021, doi:10.1109/PIERS53385.2021.9694896.

[70] R. C. Guido, "Wavelets behind the scenes: Practical aspects, insights, and perspectives," *Physics Reports*, vol. 985, pp. 1-23, 2022, doi: 10.1016/j.physrep.2022.08.001.

[71] S. Arfaoui, A. B. Mabrouk, and C. Cattani, "Wavelet analysis: basic concepts and applications," *Chapman and hall/CRC*, 2021, doi: 10.1201/9781003096924.

[72] C. Lastre-Domínguez, Y. S. Shmaliy, O. Ibarra-Manzano, J. Munoz-Minjares, and L. J. Morales-Mendoza, "ECG signal denoising and features extraction using unbiased FIR smoothing," *BioMed research international*, vol. 2019, p. 2608547, 2019, doi:10.1155/2019/2608547.

[73] A. John, J. Sadasivan, and C. S. Seelamantula, "Adaptive Savitzky-Golay filtering in non-Gaussian noise," *IEEE Transactions on Signal Processing*, vol. 69, pp. 5021-5036, 2021, 10.1109/TSP.2021.3106450.

[74] J. Dombi and A. Dineva, "Adaptive Savitzky-Golay filtering and its applications," *International Journal of Advanced Intelligence Paradigms*, vol. 16, no. 2, pp.145-156, 2020, doi:10.1504/IJAIP.2020.107011.

[75] N. B. Gallagher, "Savitzky-Golay smoothing and differentiation filter," *Eigenvector Research Incorporated*, 2020, doi: 10.13140/RG.2.2.20339.50725.

[76] P. E. McSharry, G. D. Clifford, L. Tarassenko, and L. A. Smith, "A dynamical model for generating synthetic electrocardiogram signals," *IEEE Transactions on Biomedical Engineering*, vol. 50, no. 3, pp. 289-294, 2003, doi:10.1109/TBME.2003.808805.

[77] J. J. A. Mendes Junior, D. P. Campos, L. C. D. A. V. D. Biassio, P. C. Passos, P. B. Júnior, A. E. Lazzaretti, and E. Krueger, "AD8232 to biopotentials sensors: Open source project and benchmark," *Electronics*, vol. 12, no. 4, p. 833, 2023, doi:10.3390/electronics12040833.

[78] Texas Instruments. *ADS111x ultra-small, low-power, I2C-compatible, 860-SPS, 16 bit ADCs with internal reference, oscillator, and programmable comparator data sheet*. Texas Instruments, 2009.

[79] Texas Instrument. *Analog Front-End Design for ECG Systems Using Delta-Sigma ADCs*. Application Report, SBAA160A, 2009.

[80] Y. Gan, W. Rahajandraibe, R. Vauche, B. Ravelo, N. Lorriere, and R. Bouchakour, "A new method to reduce motion artifact in electrocardiogram based on an innovative skin-electrode impedance model," *Biomedical Signal Processing and Control*, vol. 76, p. 103640, 2022, doi: 10.1016/j.bspc.2022.103640.